CHAPTER 4 – TOP NOTCH SIZE CLASSIFICATION USING 'SECONDARY' REFLECTED AND TRANSMITTED SIGNALS

4.1 Background

Prior work has shown the means of generating 'leaky' Rayleigh waves about a cylindrical hole and the subsequent measurement of the resulting circumferential body waves propagating from the hole to determine the existence of surface breaking cracks [16]. In addition to detection, it would be desirable to also classify cracks according to size. Accurate determination of the crack length would be valuable toward selecting the required diameter to resize the hole in order to remove the flaw and possibly streamlining the process for the addition of a patch or replacement of a panel section.

Considerable research has examined the scattering of waves from a surface-breaking crack on an elastic half-space [42-46]. The analysis performed by Nagy et al [16] of the inspection capability of surface breaking cracks on a cylindrical cavity by a leaky Rayleigh wave used results from these studies to estimate the crack length detection performance. A linear relation between the reflection coefficient for an incident surface wave and crack length exists for small cracks sizes [42]. For the weep hole case, it was determine that sizing could be performed for top cracks smaller than 0.020" (about one wavelength of the creeping Rayleigh wave) [16]. For larger crack

lengths, saturation of the magnitude for both the primary reflected waves and the relative difference between the reflected and transmitted waves was found.

For successful sizing of top cracks larger than 0.020 in., information in addition to the magnitude of the reflected and transmitted 'leaky' Rayleigh waves is required. One obvious source for additional signals would be the diffraction from the crack tip. Figure 4.1 shows experimental results for the pulse-echo transducer response for three weep hole conditions: no-notch, 0.063 in. top notch, and 0.145 in. tip notch. For the notch cases, following the primary reflected circumferential Rayleigh wave signal, there exists secondary reflected signals. For the 0.063 in. top notch, the secondary signal is superimposed on the end of the primary reflected signal. For the 0.145 in. top notch, the secondary signal is clearly separated further in time from the primary reflected signal. This location in time of the secondary signals may be used to classify the length of a top crack. Due to the curvature of the weep hole, the signals that are incident upon the crack tip will be considerably different from the case of a flat surface. This difference can be contributed to the 'leaking' of the Rayleigh wave as it propagates about the curved surface. In order to develop a broader understanding of the scattering phenomenon desired for sizing purposes, curved surface models must be investigated.

The problem of Rayleigh wave propagation on cylindrical surfaces was solved by Rulf [47]. Budreck presented work on the ultrasonic scattering for a cylindrical hole containing a half-penny shape crack [48]. Budreck formulated this problem using a Born series solution in crack-opening displacement exact to first order. The calculated crack-

opening displacement was used to compute the Auld voltages differentials, which are related to the difference in transducer voltage due to backscatter of the crack to the no-crack case. However, this work does not directly describe the nature of the scattering by surface waves incident to a surface-breaking crack. Also, due to the Born approximation, secondary reflections between the cavity and the crack are not properly handled. No other work has been found for the case of the scattering of a Rayleigh wave from a surface-breaking crack located on a curved surface.

The focus of this chapter is to develop a better understanding through modeling of the nature of the scattering from a surface breaking crack on a cylindrical hole. Ray analysis, analytic models and boundary element method (BEM) simulations were explored to characterize the 'secondary' reflected and transmitted signals from cracks on a cylindrical hole. From this understanding, scenarios for the sizing of surface breaking cracks on a cylindrical hole are proposed.

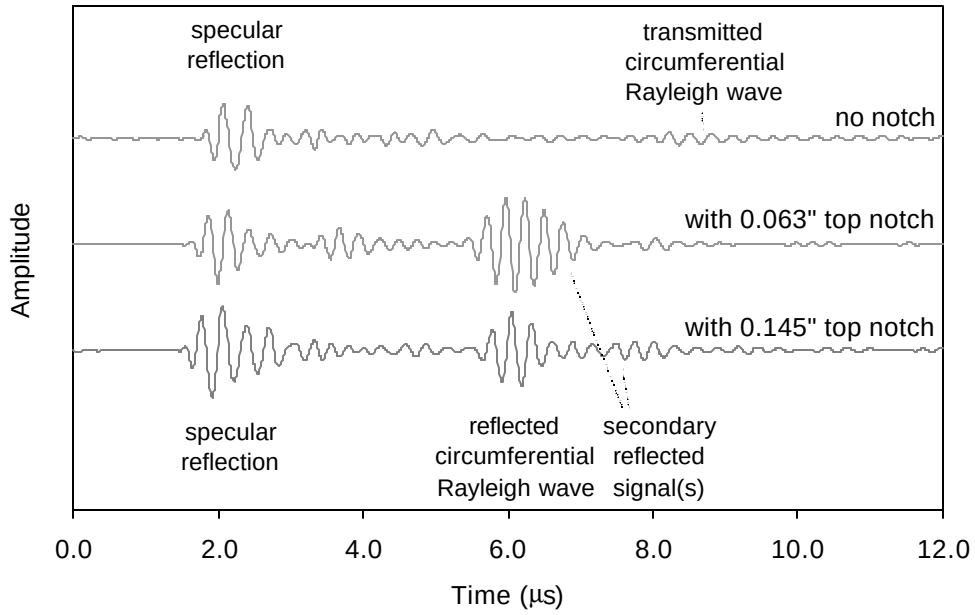

Figure 4.1. Experimental pulse-echo transducer signals

4.2 Ray Theory Analysis of Secondary Reflected Signals by a Surface Breaking Crack on a Cylindrical Hole from an Incident 'Leaky' Rayleigh Wave

A ray analysis of the time of flight can offer insight into the source of secondary signals. Figure 4.2 displays a geometric diagram used for the time of flight analysis. The time of flight to travel from and return to point A via reflection of the Rayleigh wave by the crack mouth (path ABA), by the generation of the circumferential wave which is diffracted by the crack tip and transmitted back to point A (path ACA), by the generation

of the circumferential wave which is diffracted by the crack tip and transmitted across the crack mouth (path ACBA or conversely path ABCA), and for transmission of the Rayleigh wave by the crack mouth followed by diffraction at the crack tip back along the crack and transmission back across the crack mouth (path ABCBA) are given, respectively, by

$$\tau_{ABA} = \frac{2s}{c_{r'}}, \tag{4.1}$$

$$\tau_{ACA} = \frac{2b}{c_t}, \tag{4.2}$$

$$\tau_{ACBA} = \tau_{ABCA} = \frac{b}{c_t} + \frac{l}{c_r} + \frac{s}{c_{r'}}, \tag{4.3}$$

$$\tau_{ABCBA} = \frac{2s}{c_{r'}} + \frac{2l}{c_r}, \tag{4.4}$$

where c_t is the phase velocity of shear waves (~3130 m/s in Al), c_r is the phase velocity of Rayleigh waves (~2897 m/s in Al), $c_{r'}$ is the phase velocity of leaky Rayleigh waves on a cylindrical cavity (~2752 m/s in Al at 5.0 MHz), a is the radius of cylindrical hole (0.125 in.), l is the length of the crack, s is the arc length of path AB and b is the distance of propagation by the circumferential wave to the crack tip. The lengths s and b can be expressed by the following relations respectively

$$s = aCos^{-1}\left(\frac{1}{1+\zeta}\right), \tag{4.5}$$

$$b = a\sqrt{\zeta^2 + 2\zeta}\ , \tag{4.6}$$

where $\zeta = \frac{l}{a}$. Of interest is the difference in time of flight from the main reflected leaky Rayleigh wave signal by the three following signals. These three time of flight differences are given by

$$\Delta t_1 = t_{ACA} - t_{ABA} = \frac{2b}{c_t} - \frac{2s}{c_{r'}}, \tag{4.7}$$

$$\Delta t_2 = t_{ACBA} - t_{ABA} = \frac{b}{c_t} + \frac{l}{c_r} - \frac{s}{c_{r'}}, \tag{4.8}$$

$$\Delta t_3 = t_{ABCBA} - t_{ABA} = \frac{2l}{c_r}. \tag{4.9}$$

One note from these three equations is that the time of flight difference for the two diffracted circumferential waves from the crack tip ($\Delta\tau_1$ and $\Delta\tau_2$) are functions of the curvature of the hole while the time of flight difference for the reflected Rayleigh wave from the crack tip ($\Delta\tau_3$) is not.

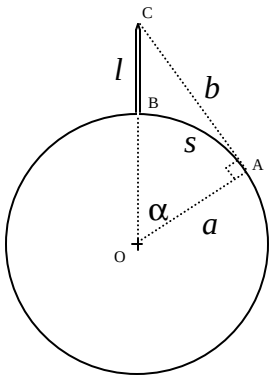

Figure 4.2. Travel paths for the geometry of a cylindrical hole with a surface breaking crack.

Figure 4.3 displays a plot of the three time of flight differences with respect to the nondimensionalized crack length. Clearly, the plot indicates the lower time of flight difference for the two diffracted circumferential waves from the crack tip versus the reflected Rayleigh waves from the crack tip. Table 4.1 lists the time of flight difference for a few example crack length cases. When considering the 0.063 in. notch results with the experimental signals in Figure 4.1, it is very difficult to separate these 'secondary' signals from the primary reflection due to the width of the transient pulse. The 'secondary' signals seem to be superimposed on the tail end of the primary reflection, which correlates with expected time of flight difference of 0.33 and 0.72 μsec for the first two secondary signals. For the 0.145 in. notch case, the first two secondary signals seems to contribute to a combined secondary signal following the initial reflection, at 1.37 and 1.96 μsec. By comparing the calculated time of flights with the experimental

results, the first two secondary waves seem to be the major contributors to the observed secondary pulse. In order to better understand the magnitude to which these waves contribute to the secondary signals, additional modeling is still needed.

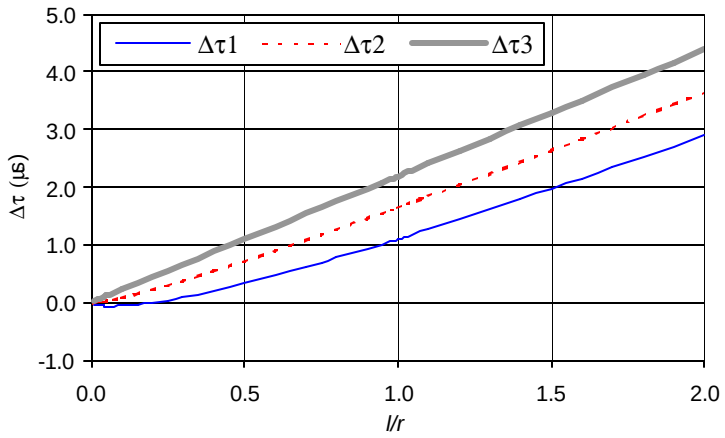

Figure 4.3. Diagram of time differences for the geometry of a cylindrical hole with a surface breaking crack.

Table 4.1. Time of flight differences for the geometry of a cylindrical hole with a surface breaking crack.

L	$\Delta\tau_1$	Δt_2	Δt_3
(in)	(μsec)	(μsec)	(μsec)
0.063	0.33	0.72	1.10
0.105	0.83	1.34	1.84
0.145	1.37	1.96	2.54

4.3 Analytic Analysis of Scattering By an Incident Shear Plane Wave from a Cylindrical Hole

To determine the magnitude of the first and second 'secondary' reflected signals, results for the magnitude of an incident field incorporating the 'leaky' Rayleigh wave at the crack tip can be used. An estimate for the shear transducer case can be obtained by calculating the analytic solution for an incident shear plane wave on a cylindrical hole. The goal of this investigation is to calculate the analytic solution for the response at possible top-crack tip locations on a cylindrical hole. With this solution, an estimate of the magnitude of the diffracted wave as a function of notch length can be made.

Figure 4.4 displays a diagram for the analytic model with an 'imaginary' top notch with the tip location at point C. The analytic solution for an incident shear plane wave on a cylindrical hole was derived by Mow and Mente [49]. The incident transient signal and the corresponding frequency signal representing a typical inspection transducer are shown in Figures 4.5(a) and 4.5(b) respectively. This analytic transient analysis approach was also used by Nagy et al to investigate the fluid-filled hole case [20].

Figure 4.6 shows the total field in-plane deflection magnitude at the imaginary notch tip for different notch lengths and selected normalized hole diameters with respect to wavelength. The value for d/λ of 10.1 corresponds to the typical inspection case with a weep hole diameter of 0.250 in. and transducer center frequency of 5.0 MHz. Clearly,

there exists a significant variation in the magnitude of the incident signal at the notch tip with variation in notch length. A significant reduction and a subsequent increase in the magnitude of the signal at the notch tip for increasing notch length is predominantly due to the destructive and constructive interference of the incident and specularly reflected signals with the 'leaky' Rayleigh wave signal. This result indicates that the magnitude of the first and second 'secondary' reflected signals may become reduced for smaller notch lengths and increased for larger notch lengths.

Figure 4.7 shows the peak-to-peak magnitude of an incident 'leaky' Rayleigh wave that has traveled about the weep hole from the opposite side from the notch. This plot displays the magnitude of the field at the notch tip due only to an incident 'leaky' Rayleigh wave. As expected, as the notch length increases, the magnitude at the notch tip decays. It can be observed that higher frequency signals more readily hold near the hole surface at this location and thus produce somewhat less response away from the hole.

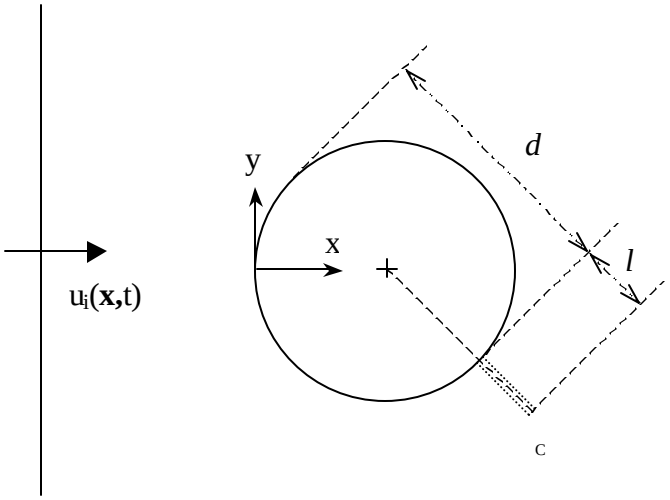

Figure 4.4. Geometry for cylindrical hole with location of imaginary notch and an incident plane shear wave.

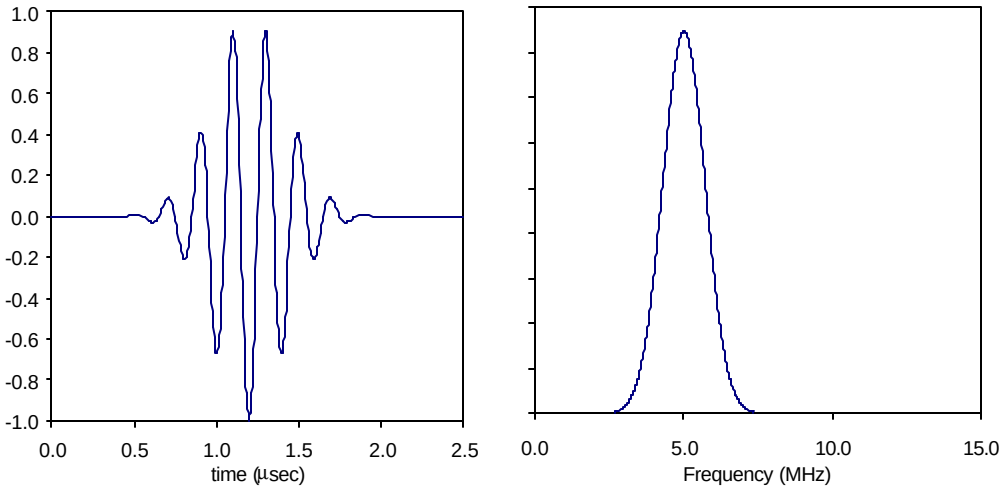

Figure 4.5. Transient pulse (a) in time domain, and (b) frequency spectrum.

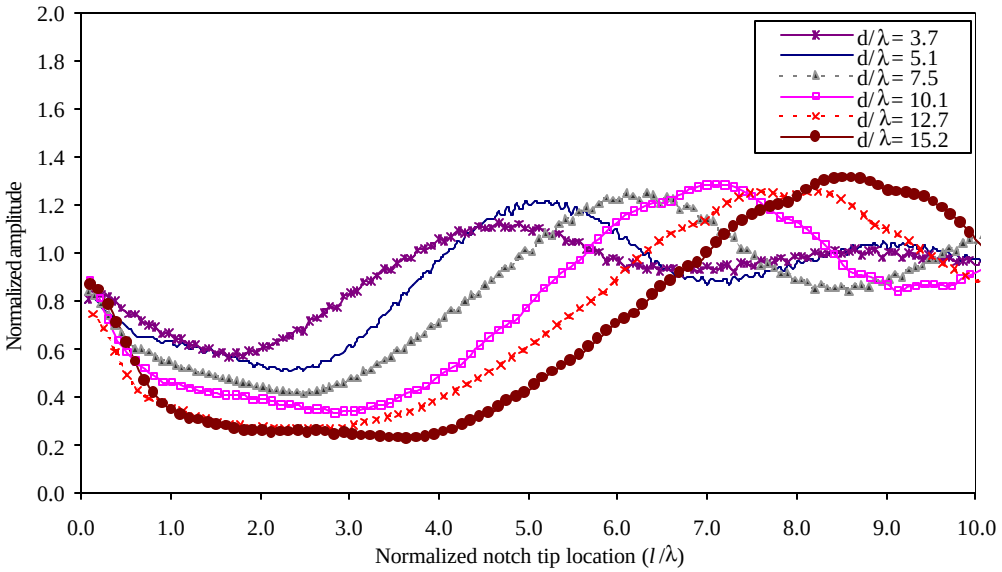

Figure 4.6. Magnitude of response at 'notch tip' due to an incident plane shear wave.

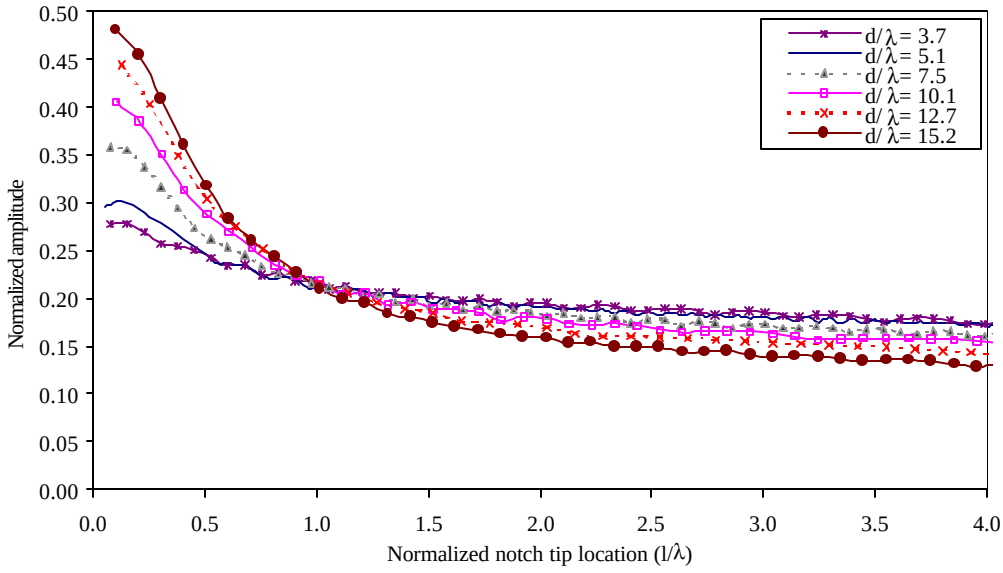

Figure 4.7. Magnitude of response at 'notch tip' due to the circumferential 'creeping' Rayleigh wave.

4.4 BEM Simulations of the Scattering By Incident Transducer Signal from a Cylindrical Hole

To best understand the complex scattering from a cylindrical hole with a surface breaking notch for an incident transducer field, numerical simulations are needed. Figure 4.8 shows a diagram for the incident transducer response case. A BEM simulation was previously developed by Aldrin et al [23] and results have been shown in previous chapters. The parameter settings for this study are given in Appendix A.

First, the peak-to-peak response at point C for the no-notch case was examined in a similar way as in the previous section, but for an incident transducer signal representing in-field conditions. Figure 4.9 shows the peak-to-peak response at the imaginary notch tip for different notch lengths and selected transducer frequencies. Again, there exists a significant variation in the magnitude of the incident signal at the notch tip depending on the notch length. This variation is predominantly due to interference between the incident wave, the specular reflection, and the generated 'leaky' Rayleigh wave on the cylindrical hole. Thus, the lower response for notch sizes from 0.030 to 0.080 in. will produce less significant secondary signals, while the higher response for notch sizes from 0.120 to 0.200 in. will likely produce more significant signals. This result may indicate a significant challenge for a size classification algorithm for notch lengths from 0.030 to 0.080 in.

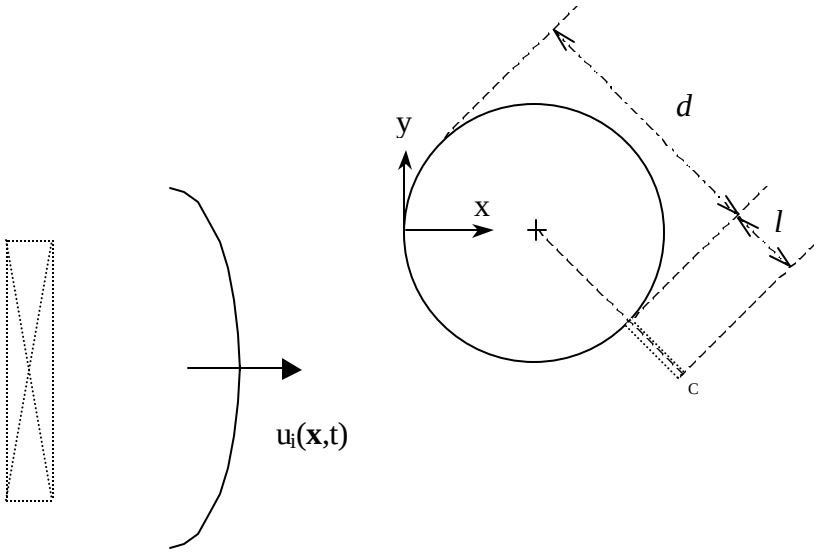

Figure 4.8. Geometry for cylindrical hole with location of imaginary notch and an incident shear wave generated by a transducer.

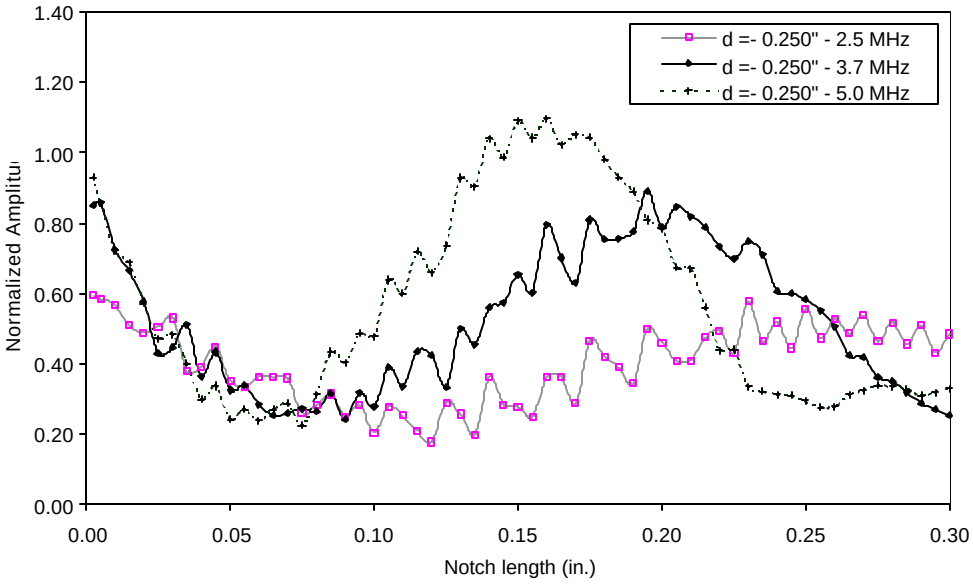

Figure 4.9. Magnitude of response at 'notch tip' due to an incident transducer signal.

4.5 BEM Simulations of the Reflected and Transmitted Signals from Notch on Cylindrical Hole

A second analysis using the BEM model examined the reflection and transmission about an actual notch on a cylindrical hole for an incident transducer signal. Figure 4.10 shows a diagram of the inspection case. In order to properly compare the reflection and transmission results for various notch lengths, the response at locations A', for reflection from the notch, and E', for transmission across the notch, were examined. These two locations will allow the diffracted wave from the notch tip (point C) to return to the hole and generate a surface wave for all possible crack lengths. At these locations, the R/T ratio (peak-to-peak at A' / peak-to-peak E') was calculated. These calculations were used to assess magnitude trends of the 'primary' reflected and transmitted signals.

Figure 4.11 displays the peak amplitude for the 'primary' reflected and transmitted signals from a notch on a cylindrical hole for three transducer frequencies. Saturation of the reflected signals between 0.010 to 0.020 in. agrees with results for both the analytic solution for the flat surface case and for the experimental results presented by Nagy [16]. The peak reflected signal settles to a constant magnitude for larger notch sizes. The general trend for the peak transmitted signal is a rapid decrease up to notch sizes of around 0.015 in. followed by a more gradual decay with significant fluctuation. This gradual decay correlates with an increased travel path for larger notch lengths where geometric decay of the transmitted signal from the notch tip occurs. Since the

transmitted signal is propagating from the notch tip, the time of flight for this signal may be used for notch sizing. The observed fluctuations can be contributed to the varying interference of the incident signals at the notch tip at point C (such as the incident transducer, specular reflection, and 'leaky' Rayleigh wave signals), and the varying interference of multiple transmitted signals at point E (such as paths ACE, ACDE, ABCE and ABCDE) for changes in notch length. These general trends seem to hold for the three transducer frequencies investigated.

Figure 4.12 displays the R/T ratio calculated for various notch lengths and for three transducer frequencies. The general trend for the R/T ratio is an increase for larger notch lengths with considerable fluctuation superimposed. These fluctuations result from the calculated fluctuations in the transmitted signal. Direct use of the R/T measure is unlikely over a wide notch length range. Although the R/T curve cannot be used directly to infer notch length, it again indicates that the transmitted signals are decaying due to increased travel for larger notch sizes.

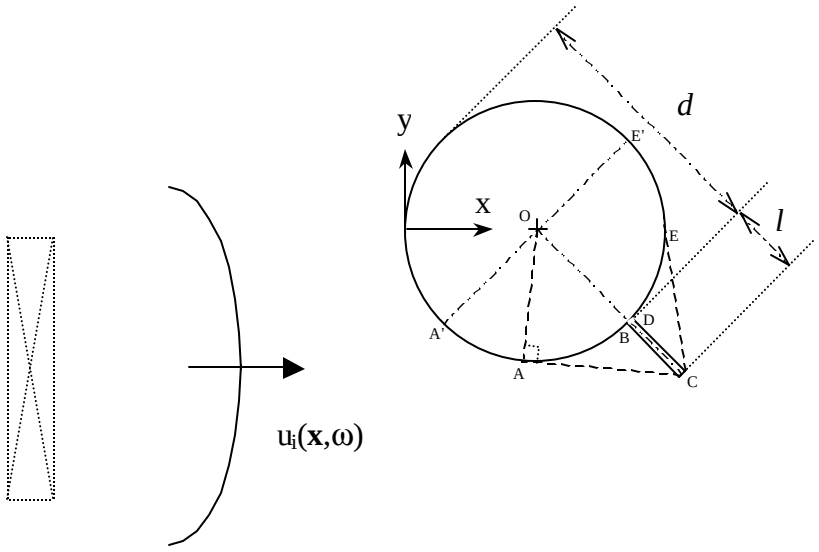

Figure 4.10. Geometry for a cylindrical hole with a surface breaking crack.

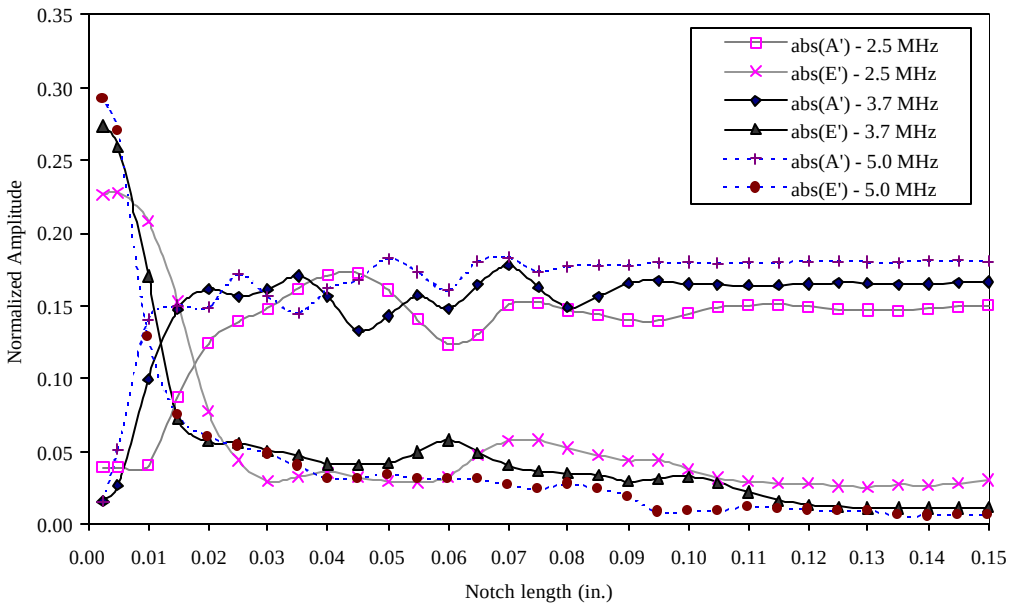

Figure 4.11. Response for points A' and E' due to an incident transducer signal.

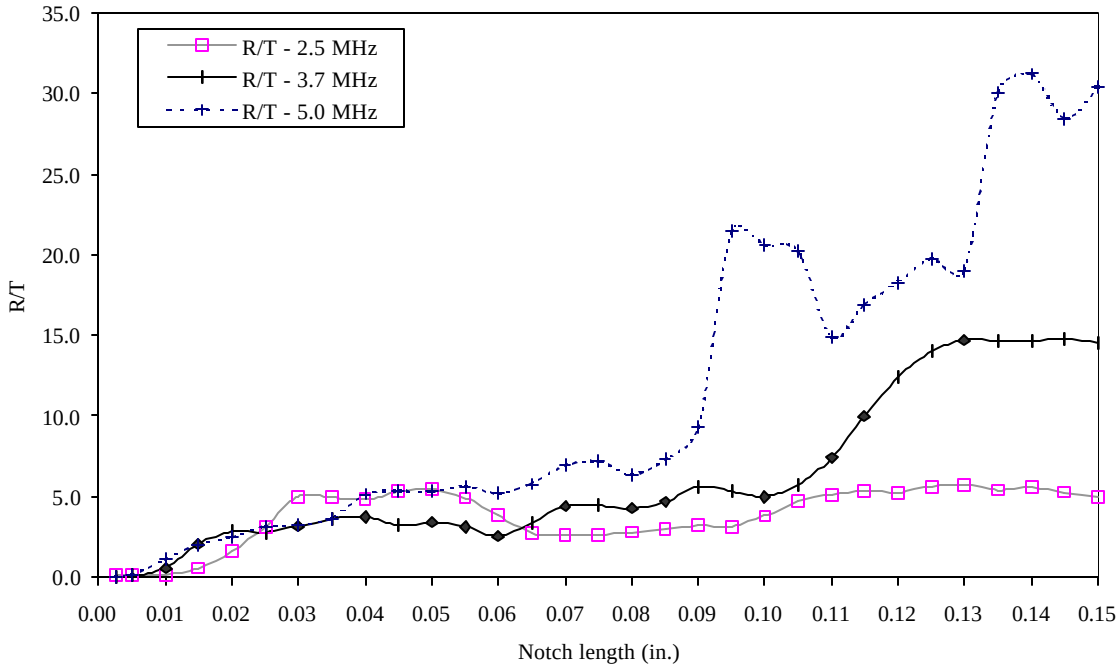

Figure 4.12. R/T ratio due to an incident transducer signal.

4.6 BEM Simulations of Transducer Signals and Discussion of Inspection Procedure

A third analysis incorporating the BEM model will examine the pulse-echo and pitch-catch transducer responses from a cylindrical hole with a top notch. The goal of this analysis is to use all of the prior studies in conjunction with these simulated transducer signals to better understand the nature of the 'secondary' reflected and transmitted signals. Through this understanding, an approach for top notch size classification will be developed.

Figure 4.13 shows the pulse-echo transducer response for a range of top notch lengths from 0.005 to 0.150 in. The theoretical time of flight calculations by the ray method for the three secondary reflected signals discussed in Section 4.2 are also plotted on Figure 4.13. The first and second 'secondary' reflected signals can clearly be observed for larger notch lengths (0.070 in. and larger). The ray method calculation for the time of flight for these two signals matches fairly well with the BEM simulation results. In general, the first 'secondary' reflected signal is about twice as large as the second 'secondary' reflected signal. Due to the close proximity of these signals, they will both participate in any proposed classification algorithm. For the cases of a notch varying between 0.030 in. and 0.070 in., the magnitude of the 'secondary' signals is both degraded and hidden within the primary reflection signal. This observation corresponds

with the results presented in Section 4.3 and 4.4. Clearly, the third 'secondary' reflected signal does not make a significant contribution to the measured response.

Figure 4.14 shows the pitch-catch transducer response for a range of top notch lengths from 0.005 to 0.150 inches. The three time of flight calculations presented in Section 4.2 can also be used to evaluate the nature of the transmitted signals across the notch on a cylindrical cavity. Path ACE corresponds with the first time-of-flight difference calculation. Both paths ACDE and ABCE correspond to the second time-of-flight calculation. Path ABCDE, the typical transmission path for the flat surface case, corresponds with the third time-of-flight difference calculation. The first and second transmitted signals from the notch tip can clearly be observed. The ray method calculation for the time of flight for these two signals generally matches with the BEM simulation results. Again due to the close proximity of these two signals, they will both participate in any proposed classification algorithm.

Figure 4.15 compares the BEM results with experimental data previous shown in Figure 4.1. Two notch cases, 0.063 and 0.145 in. were compared. For the 0.063 in. case, the 'secondary' reflected signal, found at the end of the primary reflected signal, is modeled. For the 0.145 in. case, the magnitude and approximate location in the time domain of the separate 'secondary' signals is also modeled. These results indicate that the analysis presented here does a sufficient job of modeling these limited experimental results. However, due to the location of the 'secondary' reflected signal with respect to

the ‘primary’ reflected signal, it may be difficult to use the signal for classification purposes.

Figures 4.16 and 4.17 show pulse-echo and pitch-catch transducer signals for the challenging classification notch lengths varying from 0.030 to 0.070 in. Although measurable, there exist only small changes due to ‘secondary’ reflected signals for the pulse-echo case. These signals are superimposed with the ‘primary’ specular reflection and may be difficult to classify. Slight variation in the shape of the ‘primary’ reflected signal or noise in the experimental measurement may obscure these signals. However for the pitch-catch signals, the transmitted signals from the notch tip experience measurable time of flight shifts with increased notch lengths. These transmitted signals are more likely to be candidates for a successful size classification routine, within the notch ranges of 0.030 and 0.070 in. Over the entire range of notch lengths, a classification algorithm should incorporate both of these signals. Following extraction of these two feature signals, neural networks have been shown to be a means of classifying the pulse shape of a signal, see Aldrin et al [23].

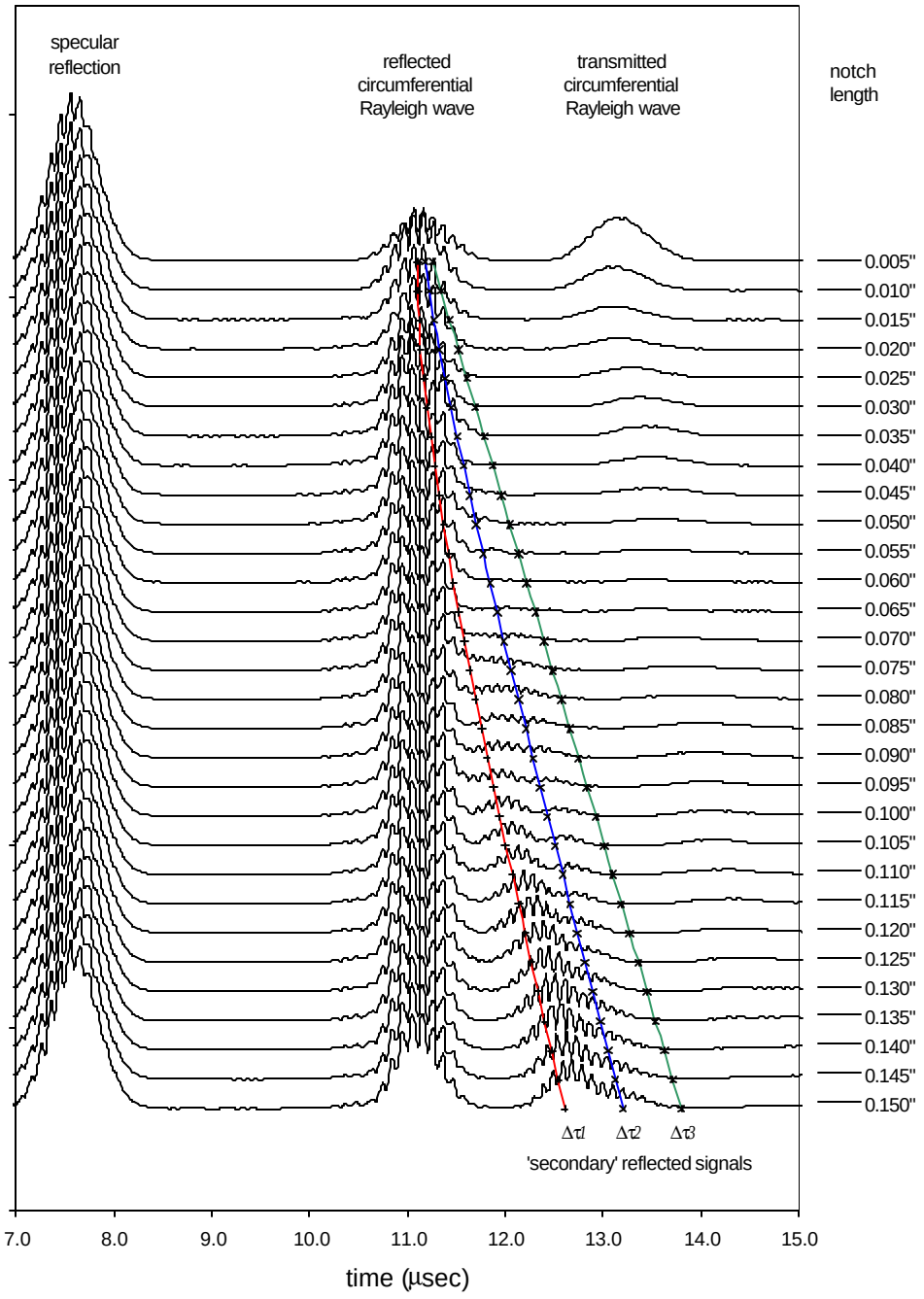

Figure 4.13. Simulated pulse-echo signals for various notch sizes.

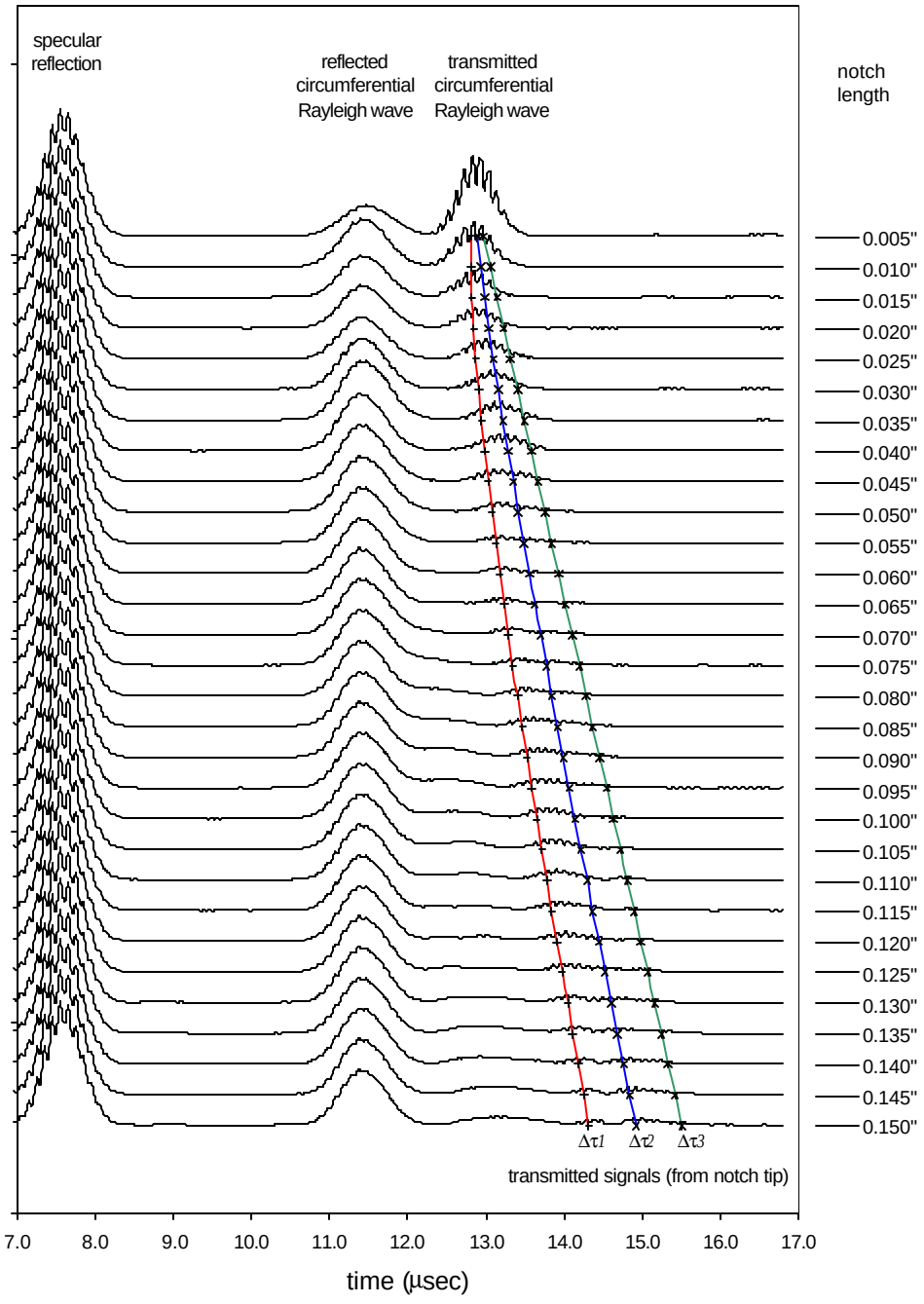

Figure 4.14. Simulated pitch-catch signals for various notch sizes.

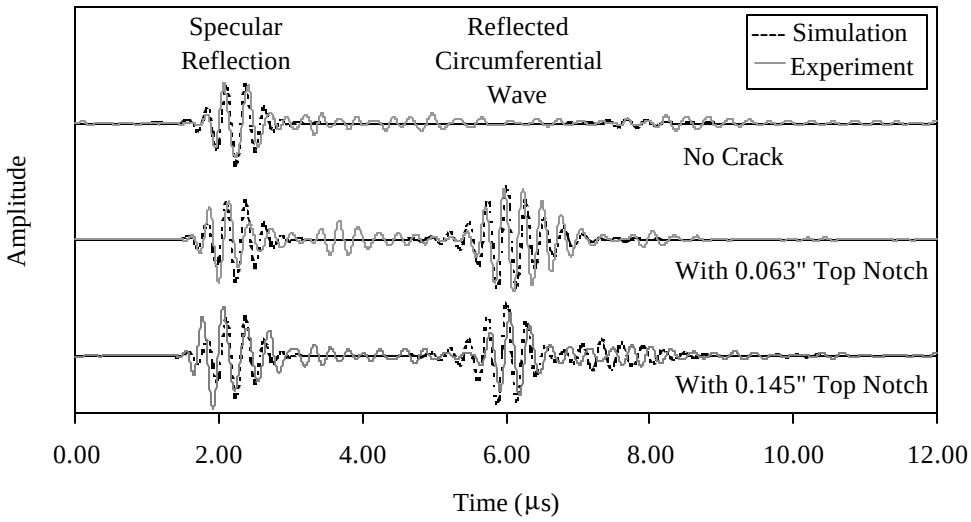

Figure 4.15. Comparison of experimental and simulated pulse echo transducer signals.

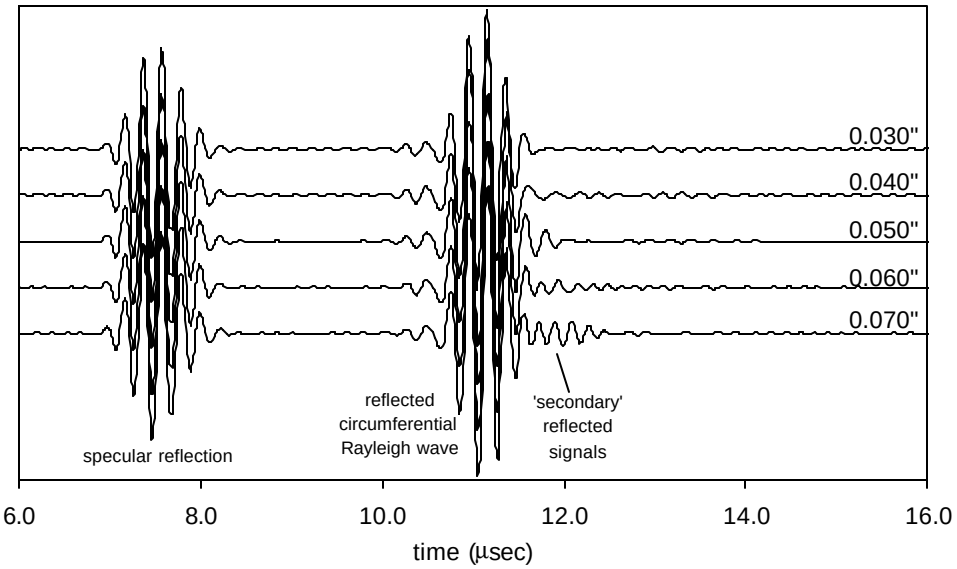

Figure 4.16. Simulated signals for the pulse-echo case for notch sizes from 0.030 to 0.070 in.

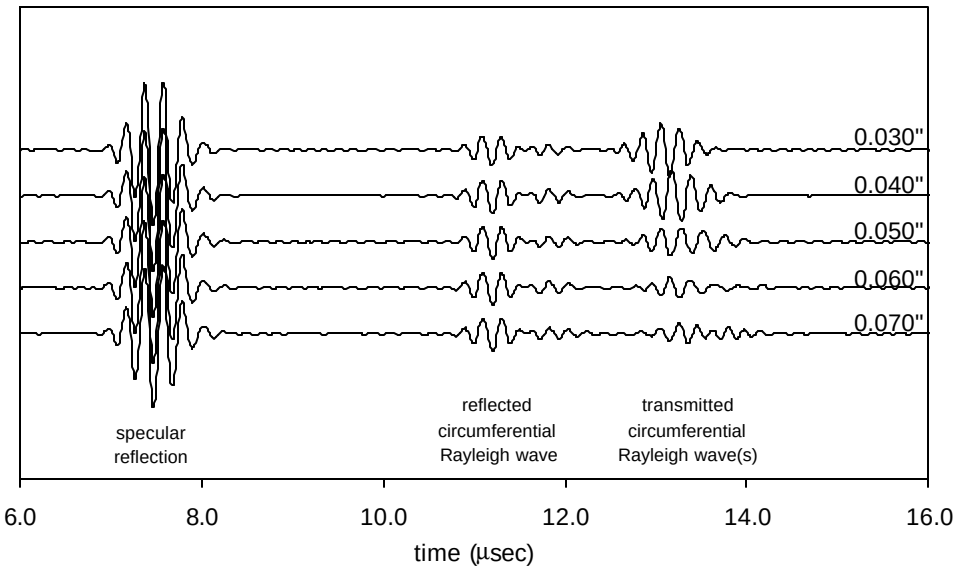

Figure 4.17. Simulated signals for the pitch-catch case for notch sizes from 0.030 to 0.070 in.

4.7 Remaining Challenges

This work is a step toward implementing an automated weep hole top-crack size classification scheme. The following are a list of issues that must be addressed to further improve a procedure that can be implemented for the C-141 weep hole case:

- transducer beam width and transient pulse shape variation expected in the field,
- 'noise' due to signals from sidewall reflections,
- variation in weep hole diameter,
- variation in weep hole depth,
- crack tip response versus response from end of EDM notches,
- variation in location of crack on hole,
- possible skew angle of crack,
- closed cracks or roughness at interface of crack,
- corner cracks (variation in depth along the width of the riser).

In order to address all of these valid issues, more information is needed concerning the expected variation for each of these parameters. The degree to which some of these parameters contribute to noise in the signals must also be further understood. For some of these parameters, such as the characteristics of the crack, further modeling and experimentation is necessary to understand their effect on the inspection procedure. Parameters such as hole depth, hole diameter, and variation in location of crack on the hole may be calculated from the ultrasonic signals. Separate

algorithms may be developed to handle these variables which can be measured during classification. An algorithm incorporating a broader array of the available A-scan data may be able to address issues such as corner cracks.

A preliminary algorithm for size classification of top notches is presented in Figure 4.18. Although the size classification have met with positive results, there still exist is a significant amount of work that must be performed in order to further optimize and subsequently validate this procedure for in-field inspection.

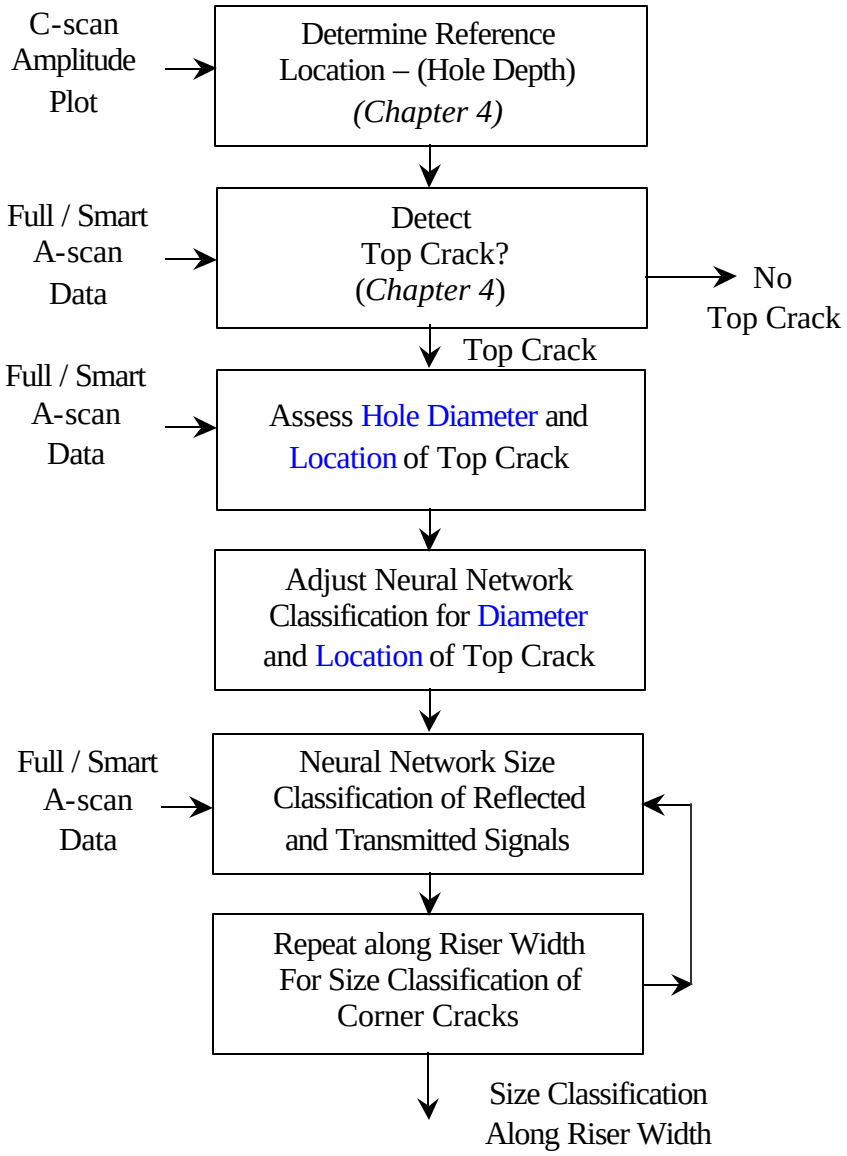

Figure 4.18. Diagram of proposed top crack size classification algorithm.